Macromolecules

pubs.acs.org/Macromolecules Article

Diffusion of a Polymer Tracer in an Unentangled Matrix

Nuofei Jiang*

Cite This: https://doi.org/10.1021/acs.macromol.5c02590 Read Online

ACCESS | Metrics & More | Article Recommendations | Supporting Information

ABSTRACT: It has been recognized for some years but remains controversial that hydrodynamic interactions are in fact not screened beyond the monomeric scale in polymer melts. This study adapts the so-called viscoelastic hydrodynamic interaction (VHI) effect to explain the center-of-mass (c.m.) diffusion of a polymer tracer of length N_{tra} diluted in an unentangled matrix of the same chemistry but different chain length N_{mat}, which disproves the classic Rouse model from the existing experimental data. The theory of the matrix effect on the tracer's c.m. diffusion is introduced, which decouples the total diffusion into the localized and hydrodynamic parts. The localized contribution is described from the diffusion of a monomer tracer in the same matrix. The time-dependent generalized Oseen tensor is used to predict the hydrodynamic contribution. The theory predicts that before the Fickian diffusion regime, the profile of the transient hydrodynamic diffusion constant relies on the parameter $N_{mat}/N_{tra}^{1/3}$. Subdiffusion is predicted to occur when $N_{mat}/N_{tra}^{1/3} \gg 1$ until the matrix relaxation time. The total diffusion constant in the Fickian regime superposes Rouse-like and Zimm-like processes. Momentum-conserving molecular dynamics simulations that cover the entire range of unentangled polymers are performed, and they show excellent agreement with theoretical predictions. The tracer's monomeric diffusion and a discussion on the nonmomentum-conserving dynamics coupled with a Langevin damping effect further support the VHI theory.

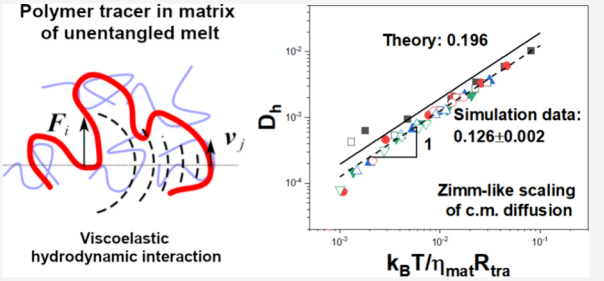

I. INTRODUCTION

The dynamics of a polymer tracer of length N_{tra} diluted in a matrix of the same chemistry but different chain length N_{mat} not only play an essential role in understanding the rheology of polydisperse samples,[1] but also provide invaluable insights into the nature of multichain interactions.[2−5] One of the most straightforward ways to tailor the matrix effect is to measure the center-of-mass (c.m.) diffusion constant of the tracer chain D_{tra}. Abundant experiments,[6−9] theories,[10−14] and computer simulations[15−17] have been reported on this subject and have initiated extensive discussions.

Tracer's diffusion depends on the relative size of the tracer and the matrix chains, as well as their comparison with the entanglement length N_e. When either the tracer or the matrix chains are below the entanglement length, there will be no topological interaction. In the unentangled regime, the diffusion of a very long tracer in a short-chain matrix is dominated by the hydrodynamic interaction (HI). This regime is also known as the Zimm regime. The tracer's c.m. diffusion constant can be expressed as

$$D_{tra}^{(Z)} \cong \frac{k_B T}{R_{tra}\eta_{mat}} \tag{1}$$

where $R_{tra}\sim N_{tra}^{\nu}$ is the size of the tracer chain, and η_{mat} is the matrix viscosity. The above expression is also known as the Stokes−Einstein (SE) relation. The tracer's dimensional exponent is equal to $\nu = 0.588$ for good solvent and $\nu = 0.5$ for θ solvent, depending on the effective intrachain excluded volume (EV) interaction. The crossover from a good solvent to a θ solvent with the increase of matrix chain length is governed by the factor $N_{mat}/N_{tra}^{1/2}$, according to the classic Flory theory.[18] That is, the matrix behaves as a θ solvent when $N_{mat} \gg N_{tra}^{1/2}$. Otherwise, it should be regarded as a good solvent. The onset of HI is thought to be consistent with the onset of EV,[11] which means eqn 1 is valid when $N_{mat} \ll N_{tra}^{1/2}$. Thus, this regime is also called the swollen hydrodynamic Stokes (SHS) regime.[11]

In the other case of $N_{mat} \gg N_{tra}^{1/2}$, HI is thought to be screened, and the tracer is expected to follow the Rouse dynamics. The self-diffusion of a monodisperse unentangled melt is a special case of this type. The corresponding tracer's diffusion constant is expressed as

$$D_{tra}^{(R)} \cong \frac{k_B T}{N_{tra}\zeta} \tag{2}$$

where ζ is the monomeric friction coefficient. In a polymer matrix, ζ depends on the distance from the glass transition

Received: September 18, 2025
Revised: November 7, 2025
Accepted: December 9, 2025

temperature T_g according to the free volume theory.[1] Thus, if the matrices of different chain lengths are maintained at temperatures having the same distance from T_g, which is the so-called iso-T_g condition, the monomeric friction coefficient is thought to be constant and the tracer's diffusion should be independent of the matrix.

Although the theoretical concept about tracer's diffusion in the unentangled regime is well recognized, a systematic validation on the crossover from the Zimm to Rouse regime is still missing. In the literature, only limited experimental data for the unentangled regime have been reported. Moreover, the existing data show significant disagreement with the theory. Green et al.[7] measured tracer's diffusion in polystyrene (PS) samples with a careful iso-T_g correction. They found that tracer's diffusion constants in unentangled matrices scale as $D_{tra}\sim N_{tra}^{-(0.5\sim 0.6)}N_{mat}^{-1}$, in agreement with the Zimm dynamics, given that $\eta_{mat}\sim N_{mat}$ for $N_{mat} < N_e$. However, they did not observe a Rouse-like regime before the onset of entanglement, where D_{tra} should be independent of N_{mat}, although their shortest tracer satisfies $N_{mat}/N_{tra}^{1/2}\gg 1$. The Rouse-like diffusion was also missing in the experimental data by Smith et al.[6] on poly(propylene oxide) (PPO), who reported $D_{tra}\sim N_{mat}^{-(0.70\sim 0.93)}$ when $N_{mat} < N_e$ and the tracer length varies from $N_{tra}\approx N_e$ to $5N_e$.

The disagreement between theory and experimental data in terms of tracer's diffusion indicates an insufficient understanding of HI in unentangled polymers. It used to be common sense that HI is negligible in polymer melt and concentrated solutions, because it is screened at the level of the concentration correlation length comparable to the size of a segment.[1,19] This concept is supported by the fact that many dynamic properties of an unentangled melt agree quite well with the Rouse model. However, in a series of publications by Farago, Semenov et al.,[20−23] it was systematically demonstrated that this concept is not correct. A new theory incorporating a time-dependent hydrodynamic effect, which is called viscoelastic hydrodynamics interaction (VHI), was raised.

The VHI theory was motivated by the anomalous transient diffusivity of unentangled polymers. For the transient mean-squared displacement (MSD): $g_3(t)\equiv\langle[\boldsymbol{R}_{c.\,m.}(t)-\boldsymbol{R}_{c.\,m.}(0)]^2\rangle$, where $\boldsymbol{R}_{c.\,m.}$ is the c.m. position of a polymer chain, the Rouse model assuming a time-independent monomeric friction coefficient predicts that the c.m. diffusion is Fickian beyond the segmental relaxation time τ_0, which means $g_3(t)\sim t$ when $t > \tau_0$. However, it is widely observed in experiments[24,25] and simulations[26] that the transient c.m. MSD contains a long-persistent subdiffusive regime before the Rouse time τ_R: $g_3(t)\sim t^{0.75\sim 0.85}$ when $\tau_0\ll t\ll\tau_R$.

This anomalous diffusion was explained by Farago, Semenov et al.[20,22] from the hydrodynamic-based mode coupling theory (hMCT) approach. They showed that in the monodisperse unentangled melt of chain length N, the hydrodynamic coupling with the viscoelastic matrix can lead to a negative tail in the c.m. velocity autocorrelation function (VAF) defined as $C_{c.\,m.}(t)\equiv\langle\boldsymbol{V}_{c.\,m.}(t)\cdot\boldsymbol{V}_{c.\,m.}(0)\rangle = 6\partial^2 g_3(t)/\partial t^2$, where $\boldsymbol{V}_{c.\,m.}$ is the c.m. velocity. This negative tail of $C_{c.\,m.}(t)$ scales as $-N^{-1/2}t^{-3/2}$ when $t\ll\tau_R$ and thus suggests the sublinear behavior: $g_3(t)\sim t^{1/2}$. It overlays with Fickian diffusion due to monomeric friction coefficient, leading to the apparent power-law exponent of $g_3(t)$ between 1/2 and 1.[22] The authors also proposed an alternative approach to account for the effects of VHI from a scale-dependent relaxation modulus and the time-dependent generalized Oseen tensor.[22,23] Their theory agrees quantitatively with the momentum-conserving molecular dynamics (MD) simulations. Besides, other evidence of long-range hydrodynamic coupling in unentangled melts has been reported. For example, the collective intermolecular motion was observed by Morhenn et al.[27] from neutron scattering. In a very recent study by Aponte-Rivera et al.,[28] the induced flow of a nanoparticle diluted in polymer melts was identified.

It was also explained[21] that although the density-based mode-coupling theory (dMCT) accounting for density fluctuation also predicts a subdiffusion regime, the amplitude of the velocity correlation function $C_{c.\,m.}(t)$ is significantly underestimated. The insufficiency of dMCT was also proved in the case of nonmomentum-conserving dynamics (Monto Carlo (MC) simulation or MD simulation coupled with a Langevin thermostat). hMCT predicts qualitatively different behaviors of $C_{c.\,m.}(t)$ from the momentum-conserving dynamics, in agreement with simulation data. However, dMCT does not predict this change.

In this study, I will explain the theory of the tracer's diffusion in unentangled matrices of different lengths after including the effect of VHI via the generalized Oseen tensor. The theory predicts that the total diffusion of a polymer tracer superposes Rouse-like and Zimm-like processes. Before reaching the Fickian diffusion regime, the transient c.m. diffusion constant as a function of time can be qualitatively different, depending on the relative value of the tracer and matrix chain lengths. Subdiffusion occurs when the matrix chain is beyond a critical length. The theoretical predictions are then compared with the momentum-conserving MD simulations based on the widely used Kremer-Grest (KG) model.[29] The discussions will cover the entire regime of unentangled polymers. The simulation data show clear evidence of the invalidity of the classic Rouse model for unentangled melts but are well consistent with the theoretical predictions based on VHI. I also extend the discussions to the nonmomentum-conserving dynamics. The VHI theory predicts a qualitatively different picture of the matrix effect on tracer's diffusion. The predictions are also supported by the MD simulations using the Langevin thermostat.

One of the main motivations for revisiting tracer's diffusion in unentangled matrix comes from recent discussions on the nonlinear extensional rheology of unentangled polymers.[30−36] A mechanism called reduction of friction coefficient has initiated extensive discussions as an explanation of the nonlinear rheology data from experiments and simulations. This mechanism accounts for the increase of chain mobility when polymers are highly aligned with each other in the melt or concentrated solutions under fast flows. For example, the steady-state extensional viscosity of an unentangled polymer melt exhibits extension-rate thickening followed by thinning.[37] The variation of extensional viscosity has been explained by a finitely extensible chain model whose monomeric friction coefficient decreases with the segmental orientation.[37,38] However, up to now, there is no predictive theory of friction reduction. In a recent study by the current author,[39] it was found that the magnitude of friction reduction under nonlinear flows agrees with the global projection area in the plane normal to the direction of stretching. It was further proposed to relate the change of mobility to the so-called reduced Kuhn density defined as the ratio of Kuhn length to packing length. However, there is still a lack of solid explanation for this phenomenological relationship.

The previous discussions about friction reduction are based on the concept that the unentangled polymers follow the Rouse

https://doi.org/10.1021/acs.macromol.5c02590
Macromolecules XXXX, XXX, XXX−XXX

dynamics assuming no HI. However, the recognition of the long-range VHI by previous studies[20−23] and further proofs from the current work indicate that the nonlinear rheology of unentangled polymers should be understood from a different standpoint. It also suggests that by incorporating the effect of VHI, it should be promising to address the remaining inconsistencies of nonlinear extensional rheology.

The rest of the paper is organized as follows: in **Section II**, the theory of tracer's c.m. diffusion in unentangled matrix is explained, accounting for VHI via the time-dependent generalized Oseen tensor. In **Section III**, the theoretical predictions are compared with momentum-conserving MD simulations. Two additional aspects are discussed in **Section IV** as further proofs of VHI in unentangled polymers: the tracer's monomeric diffusion and matrix effect on tracer's c.m diffusion in nonmomentum-conserving dynamics. The conclusions are summarized in **Section V.**

II. THEORY OF THE TRACER'S C.M. DIFFUSION IN AN UNENTANGLED MATRIX

II.1. Generalized Oseen Tensor. In this work, the effect of VHI is introduced from the generalized Oseen tensor. It starts from the generalized Navier−Stokes equation (GNSE):[22,23]

$$\rho_{mass}\frac{\partial}{\partial t}\boldsymbol{v}(\boldsymbol{r},t) = \nabla\cdot\int E_{mat}(\boldsymbol{r},t-t')\nabla\boldsymbol{v}(\boldsymbol{r},t')\mathrm{d}t' - \nabla P + \boldsymbol{f}_{ext}(\boldsymbol{r},t) \tag{3}$$

and the incompressible condition:

$$\nabla\cdot\boldsymbol{v}(\boldsymbol{r},t) = 0 \tag{4}$$

where $\boldsymbol{v}(\boldsymbol{r},t)$ is the fluid velocity. ρ_{mass} is the mass density of the fluid. P is pressure. $E_{mat}(r,t)$ is the length-scale dependent linear relaxation modulus of the matrix fluid. This concept pioneered by Brochard-Wyart and de Gennes[40] describes the response to a flow which is inhomogeneous at a length scale smaller than the matrix molecules. $\boldsymbol{f}_{ext}(\boldsymbol{r},t)$ is the external force. The integral term in the right-hand-side of eqn 3 is the viscoelastic force.

The generalized Oseen tensor $\bar{\mathcal{H}}(r,t)$ defines the linear response of the flow field to the perturbative external force acting on the fluid at $t > 0$:

$$\boldsymbol{v}(\boldsymbol{r},t) = \int\bar{\mathcal{H}}(|r-r'|,t)\cdot\boldsymbol{f}_{ext}(\boldsymbol{r}')\mathrm{d}\boldsymbol{r}' \tag{5}$$

The isotropic part of the Oseen tensor, $\mathcal{H}(r,t) = \mathrm{Tr}\bar{\mathcal{H}}(r,t)/3$, is the focus of this work.

In a simple fluid, the classic form of the Oseen tensor is widely recognized:[19]

$$\mathcal{H}(r,t) = \frac{1}{6\pi\eta_s r},\ r \leqslant l_s(t) \tag{6}$$

where η_s is the fluid viscosity. The validity of eqn 6 in the transient regime is limited by the so-called vorticity diffusion length $l_s(t)\equiv\sqrt{t\eta_s/\rho_{mass}}$. Beyond $l_s(t)$, $\mathcal{H}(r,t)$ is exponentially small. $r \leqslant l_s(t)$ can be regarded as the condition where the inertia term in the left side of eqn 3 becomes negligible. It can also be understood from the scenario of applying shear on the fluid between two plates. The shear field diffuses from the moving plates initially with a diffusion constant of η_s/ρ_{mass} until it becomes homogeneous in the fluid.

A viscoelastic fluid like a polymer melt is characterized by a time-dependent viscosity. If we look at a length scale much larger than the matrix molecules, i.e., the tracer molecule is much larger than the matrix molecule, the length-scale dependent feature of the matrix modulus can be ignored, which means $E_{mat}(r,t) \approx E_{mat}(r\to\infty,t)$. In this case, the generalized Oseen tensor can be expressed as a natural extension of its classic form:[22]

$$\mathcal{H}(r,t) = \frac{1}{6\pi\eta^*_{mat}(t)r},\ r \leqslant l^*_v(t) \tag{7}$$

where $\eta^*_{mat}(t) \equiv \int_0^t E_{mat}(r\to\infty,t')\mathrm{d}t'$ is the transient matrix viscosity at large length scales. The corresponding vorticity diffusion length changes to $l^*_v(t)\equiv\sqrt{t\eta^*_{mat}(t)/\rho_{mass}}$.

If the matrix is an unentangled melt, the transient viscosity is

$$\eta^*_{mat}(t) = \begin{cases}\eta_0(t/\tau_0)^{1/2} & \tau_0 \ll t \ll \tau_{mat}\\ \eta_{mat} & t \gg \tau_{mat}\end{cases} \tag{8}$$

where $\tau_{mat} = N^2_{mat}\tau_0$ is the Rouse relaxation time of the matrix chain. The matrix viscosity is linearly proportional to the chain length: $\eta_{mat} = N_{mat}\eta_0$, where $\eta_0 = (\rho_{mass}/m)k_BT\tau_0$ means the monomeric viscosity. Thus, the vorticity diffusion length will show two power-law regimes in terms of time: $l^*_v\sim t^{3/4}$ for $t \ll \tau_{mat}$ and $l^*_v\sim t^{1/2}$ for $t \gg \tau_{mat}$.

If the tracer is smaller than the matrix molecule, the tracer can only feel an effective viscosity up to a length scale comparable to its size.[41] Thus, in this case the global matrix viscosity in eqn 7 should be replaced by an effective viscosity $\eta^*_{eff}(t)$. For a polymer tracer with $N_{tra} \ll N_{mat}$ in the unentangled regime, it means $\eta_{eff}(t) = \eta_0(t/\tau_0)^{1/2}$ for $\tau_0 \ll t \ll \tau_{tra}$ and $\eta_{eff} \cong N_{tra}\eta_0$ for $t \gg \tau_{tra}$, where $\tau_{tra} \cong N^2_{tra}\tau_0$ is the Rouse time of the tracer.

II.2. Matrix Effect on the C.M. Diffusion of a Polymer Tracer. Using the generalized Oseen tensor, we can construct the theory of matrix effect on tracer's c.m. diffusion. Suppose that a weak perturbative force $\boldsymbol{F}$ is applied to each monomer of the tracer at $t > 0$. Due to the linearity of the Stokes flow, the velocity response is additive. Thus, the c.m. velocity can be written as

$$\langle V_{c.m.}(t)\rangle = \chi(t)\boldsymbol{F} = [\chi_l(t) + \chi_h(t)]\boldsymbol{F} \tag{9}$$

The response function $\chi(t)$ is divided into two terms: $\chi_l(t)$ for the local flow-to-force response, and $\chi_h(t)$ for the hydrodynamic contribution. The hydrodynamic part is calculated by involving all the monomer pairs via the generalized Oseen tensor:

$$\chi_h(t) = \frac{1}{N_{tra}}\sum_{\substack{i,j\\ i\neq j}}\mathcal{H}(r_{ij},t) \tag{10}$$

where $r_{ij} = |\boldsymbol{r}_i - \boldsymbol{r}_j|$ is the distance between the ith and jth monomers.

Based on the fluctuation−dissipation theorem (FDT), which imposes a rigorous relation between the flow-to-force response function and the c.m. velocity correlation function: $C_{c.m.}(t) = (k_BT/N_{tra})\partial\chi(t)/\partial t$, and the Green−Kubo relationship: $D^*_{tra}(t) = \int_0^t C_{c.m.}(t')\mathrm{d}t'$, the transient c.m. diffusion constant of a polymer tracer can be expressed as

$$D^*_{tra}(t) = \frac{k_BT}{N_{tra}}[\chi_l(t) + \chi_h(t)] \equiv D^*_l(t) + D^*_h(t) \tag{11}$$

where $D^*_l(t) \equiv k_BT\chi_l(t)/N_{tra}$ and $D^*_l(t) \equiv k_BT\chi_h(t)/N_{tra}$, respectively. The Fickian diffusion constant is the value at large times: $D_\alpha = D^*_\alpha(t\to\infty)$, where "$\alpha$" can be "*tra*", "*l*", and "*h*".

https://doi.org/10.1021/acs.macromol.5c02590
Macromolecules XXXX, XXX, XXX−XXX

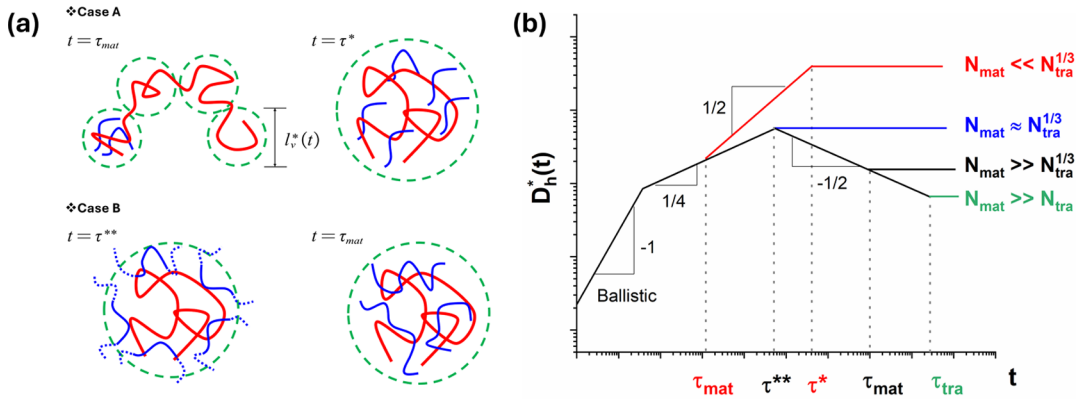

Figure 1. (a) Illustration of time-dependent hydrodynamic coupling between tracer (red) and matrix (blue) in two cases, as explained in the context. The green blobs represent the vorticity diffusion length $l_v^*(t)$. (b) Theoretical prediction on the transient hydrodynamic diffusion constant for a fixed tracer in different matrices in the unentangled regime.

Localized (Rouse-Like) Contribution. The local flow-to-force response function $\chi_l(t)$ is the inverse of monomeric friction coefficient, which depends on the effective potential acting on a monomer of the tracer. The pairwise interaction originates from intratracer and tracer-matrix interactions. The former is proportional to the density of tracer monomers inside the tracer coil, $N_{tra}/R_{tra}^3 \sim N_{tra}^{-1/2}$ for a θ solvent. Thus, the monomeric friction coefficient at long-time scales can be expressed as[21] $\zeta = \zeta_0[1 - const/(\rho N_{tra}^{1/2} b^3)]$, where ζ_0 is the monomeric friction coefficient due to tracer-matrix interaction, being the dominate factor for a long polymer tracer.

To estimate the monomeric friction coefficient of the tracer polymer, here I propose to consider a monomer tracer in the same matrix. The motions of monomer tracers are not affected by HI from other tracers in the dilute limit. A monomer tracer is trapped in a "cage" of the matrix molecules. The effective potential of the monomer tracer is not equivalent to that of a monomer in a polymer tracer in the same matrix, because in the latter case, at least two cage molecules are from the tracer chain if the monomer is not at the chain end. The monomer coordination number in a fluid is $z \approx 12$.[42] That means, after ignoring the intrachain loops, the difference between the effective potentials acting on a monomer tracer and a monomer in a polymer tracer is within a factor of $(z-2)/z$, which does not deviate much from 1. Thus, the diffusion of a monomer tracer can give a reasonable estimation of the local response function: $\chi_l(t) \approx D_{mono}^*(t)/k_BT$, and the localized contribution for a polymer tracer can be expressed as

$$D_l^*(t) = \frac{1}{N_{tra}} D_{mono}^*(t) \tag{12}$$

It represents the Rouse-like contribution to the total diffusion.

A monomer tracer can be seen as a spherical nanoparticle of small radius. Its diffusion in a polymer matrix has been extensively discussed in many studies.[41,43,44] Quantitatively successful but nonanalytical theories have been proposed.[43−45] The monomer tracer's diffusion is also time-dependent in a polymer matrix and exhibits subdiffusion, due to the slow relaxation of the memory kernel.[46] A thorough discussion on this subject is out of scope of the current work. In the rest of discussions, I will take the diffusion of a monomer tracer as a quantity to measure to account for the localized contribution of a polymer tracer. This enables us to focus on the hydrodynamic contribution which remains controversial.

In the papers by Farago, Semenov et al.,[20−23] the monomeric friction coefficient is treated as a constant without further explanation. To highlight the hydrodynamic contribution to be discussed in the following, they designed simulation models containing very long but unentangled chains by allowing chain crossing. These models showed better quantitative agreement with the theoretical predictions compared to the topology-conserving chains. In the later sections of this work, I will show that after careful estimation of the local response from the monomer tracer's diffusion, the predicted scaling behaviors of the hydrodynamic contribution can be generally observed in simulation models with finite chain length and showing a normal unentangled to entangled transition. This strategy should promise a further validation of the VHI theory from experimental data.

Hydrodynamic (Zimm-Like) Contribution. When the tracer polymer is much longer than the matrix chains, the generalized Oseen tensor is inversely proportional to the distance and the matrix viscosity, analogous to its classic form in a small-molecule solvent. Using $\mathcal{H}(r, t)$ in eqn 7, we have

$$D_h^*(t) = \frac{k_BT}{6\pi N_{tra}^2 \eta_{mat}^*(t)} \sum_{\substack{i,j \\ i \neq j}} \langle \frac{1}{r_{ij}} \rangle \tag{13}$$

It must be noted that if the matrix viscosity has no time dependence, eqn 13 is also known as the Kirkwood's expression of diffusion constant.[19]

The expression of $D_h^*(t)$ in its transient regime further relies on how the vorticity diffusion length $l_v^*(t)$, beyond which HI is negligible, compares with the tracer's size. Using $r_{ij} = |i - j|^{1/2} b$ and the preaveraging approximation, $D_h^*(t)$ can be rewritten as

$$D_h^*(t) = 0.196 \frac{k_BT}{\eta_{mat}^*(t) R_{tra}} \begin{cases} l_v^*(t)/R_{tra} & l_v^*(t) < R_{tra} \\ 1 & l_v^*(t) \geqslant R_{tra} \end{cases} \tag{14}$$

where $R_{tra} = N_{tra}^{1/2} b$ is the tracer's size. The numerical coefficient 0.196 approximates $8/3/(6\pi^3)^{1/2}$, first derived by Zimm.[47] Eqn 14 is valid when the vorticity diffusion length $l_v^*(t)$ is much larger than the Kuhn length of the tracer, $l_v^*(t) \gg b$, since it describes a nonlocal effect. For $l_v^*(t) < R_{tra}$, eq (14) is the same expression for the diffusion in a semidilute solution whose concentration correlation length is equal to $l_v^*(t)$, under the concept of hydrodynamic screening.[1] When $l_v^*(t) \geqslant R_{tra}$, eqn 14 becomes the SE relation consistent with eqn 1. Because $l_v^*(t)$ increases

https://doi.org/10.1021/acs.macromol.5c02590
Macromolecules XXXX, XXX, XXX−XXX

with time and it always become larger than tracer's size at some moment, eqn 14 returns to the Zimm model prediction at large times.

The time-dependence of the transient c.m. diffusion constant $D_h^*(t)$ needs to be considered in two cases, as illustrated in Figure 1(a).

Case A. $l_v^*(\tau_{mat}) \ll R_{tra}$, the vorticity diffusion length is still smaller than the tracer's size after the full relaxation of the matrix chains. This case corresponds:

$$N_{mat}/N_{tra}^{1/3} \ll (b^2\rho_{mass}/\eta_0\tau_0)^{1/3} \tag{15}$$

The profile of $D_h^*(t)$ as a function of time is controlled by the parameter $N_{mat}/N_{tra}^{1/3}$. This case represents the limit of small-molecule solvent. The critical time τ^* when momentum spreads the tracer's size R_{tra} is larger than the matrix chain relaxation time τ_{mat}. It is defined by $l_v^*(\tau^*) \cong \sqrt{\tau^*\eta_{mat}/\rho_{mass}} \approx R_{tra}$, which means $\tau^* \cong \rho_{mass}R_{tra}^2/\eta_{mat} \gg \tau_{mat}$. The corresponding transient c.m. diffusion constant $D_{tra}^*(t)$ is written as

$$D_h^*(t) \cong \frac{k_BT}{R_{tra}}\begin{cases} l_v^*(t)/\eta_{mat}^*(t)R_{tra} & t \ll \tau_{mat} \\ l_v^*(t)/\eta_{mat}R_{tra} & \tau_{mat} \ll t \ll \tau^* \\ 1/\eta_{mat} & t \gg \tau^* \end{cases} \tag{16}$$

At short times, $t \ll \tau_{mat}$, the transient hydrodynamic diffusion constant $D_h^*(t)$ as a function of time depends on the vorticity diffusion length $l_v^*(t)$ and the transient matrix viscosity $\eta_{mat}^*(t)$. In the intermediate time regime, $\tau_{mat} \ll t \ll \tau^*$, only the time dependence of $l_v^*(t)$ matters.

Substituting the expressions of $l_v^*(t)$ and $\eta_{mat}^*(t)$ of the corresponding regimes into eqn 16, the dependence of $D_h^*(t)$ is (omitting the chemistry-dependent parameters):

$$D_h^*(t) \sim \begin{cases} N_{tra}^{-1}t^{1/4} & t \ll \tau_{mat} \\ N_{tra}^{-1}N_{mat}^{-1/2}t^{1/2} & \tau_{mat} \ll t \ll \tau^* \\ N_{tra}^{-1/2}N_{mat}^{-1} & t \gg \tau^* \end{cases} \tag{17}$$

which means $D_h^*(t)$ increases with time monotonically. Because the transient viscosity $\eta_{mat}^*(t)$ is not well described by Rouse-like behavior when N_{mat} is small, the change in the time exponents of $D_h^*(t)$ may not be readily distinguishable from the data. However, it should be clear that the onset of Fickian diffusion is irrelevant with matrix relaxation.

Case B. $l_v^*(\tau_{mat}) \gg R_{tra}$, the vorticity diffusion length becomes comparable to tracer's size before the terminal relaxation of matrix. Correspondingly, it requires $N_{mat}/N_{tra}^{1/3} \gg (b^2\rho_{mass}/\eta_0\tau_0)^{1/3}$. In this case, the critical time τ^{**} from which the vorticity diffusion length $l_v^*(t)$ becomes comparable to the tracer's size R_{tra} is smaller than the matrix chain relaxation time τ_{mat}. It is determined by the formula: $l_v^*(\tau^{**}) \cong \sqrt{\tau^{**}\eta_{mat}^*(\tau^{**})/\rho_{mass}} \approx R_{tra}$, which gives $\tau^{**} \cong (\rho_{mass}\eta_0^{-1}\tau_0^{1/2}R_{tra}^2)^{2/3} \ll \tau_{mat}$. It is independent of matrix chain length but increases with the tracer's length. The transient c.m. diffusion constant $D_h^*(t)$ is described as

$$D_h^*(t) \cong \frac{k_BT}{R_{tra}}\begin{cases} l_v^*(t)/\eta_{mat}^*(t)R_{tra} & t \ll \tau^{**} \\ 1/\eta_{mat}^*(t) & \tau^{**} \ll t \ll \tau_{mat} \\ 1/\eta_{mat} & t \gg \tau_{mat} \end{cases} \tag{18}$$

The difference between eqns 16 and (18) for $D_h^*(t)$ lays in the intermediate times before reaching the Fickian diffusion regime. In the matrix of very short chains, the time dependence of $D_{tra}^*(t)$ depends on the vorticity diffusion length $l_v^*(t)$ which is smaller than the tracer's size. In contrast, when the matrix chain is beyond critical length, momentum has spread over the entire tracer chain by $\tau^{**} \ll \tau_{mat}$, and the slow viscoelastic relaxation of the matrix chains controls the transient diffusion of the tracer in the time window $\tau^{**} \ll t \ll \tau_{mat}$.

The time and chain length dependences of the transient hydrodynamic diffusion constant $D_h^*(t)$ is

$$D_h^*(t) \sim \begin{cases} N_{tra}^{-1}t^{1/4} & t \ll \tau^{**} \\ N_{tra}^{-1/2}t^{-1/2} & \tau^{**} \ll t \ll \tau_{mat} \\ N_{tra}^{-1/2}N_{mat}^{-1} & t \gg \tau_{mat} \end{cases} \tag{19}$$

Thus, $D_h^*(t)$ decreases with time in the regime $\tau^{**} \ll t \ll \tau_{mat}$. The exponent is close to the prediction of the tube model for entangled polymers in the regime between the entanglement time and the terminal relaxation time. However, in the unentangled regime, after superposing with the localized contribution, the total transient diffusion constant of the tracer should exhibit a weaker time dependence than predicted. Another interesting property predicted by eqn 19 is that the onset of Fickian diffusion is explicitly related to the relaxation time of the matrix chain τ_{mat}. This will be important proof of this hydrodynamic-based approach for tracer's diffusion.

When a short tracer is put into a longer matrix $N_{mat} > N_{tra}$, it is predicted that the tracer will feel an effective viscosity η_{eff} in a scale comparable to the tracer. The profile of $D_h^*(t)$ should be similar to the cases of $N_{mat} > N_{tra}^{1/3}$, but the subdiffusion regime persists up to the tracer's relaxation time τ_{tra} and no longer changes with the increase of matrix length.

The theoretical prediction for a fixed tracer in different matrices is summarized in Figure 1(b). The total diffusion constant in the Fickian regime is predicted to be the following:

$$D_{tra} = D_l + D_h = \frac{D_{mono}}{N_{tra}} + 0.196\frac{k_BT}{R_{tra}\eta_{eff}} \tag{20}$$

where $\eta_{eff} = \eta_{mat}$ for $N_{tra} \gg N_{mat}$ and $\eta_{eff} \cong N_{tra}\eta_0$ for $N_{tra} \ll N_{mat}$. The localized part is consistent with the Rouse model, $D_l \sim N_{tra}^{-1}$, given that the diffusion of the monomer tracer is constant, $D_{mono} \approx const.$ Thus, for a fixed tracer in different matrices, D_{tra} will depend on the matrix chain length N_{mat} with an exponent value between -1 (Zimm model) and 0 (Rouse model). When considering different tracers in the same matrix, D_{tra} should depend on the tracer's size R_{tra} with an exponent value between -2 and -1. With the increase of tracer chain length or the decrease of matrix chain length, the hydrodynamic contribution will become more important, and thus, the tracer's diffusion will be more Zimm-like.

Given that the localized contribution can be affected by the nonbond potential between monomers and by the distance to the glass transition, the observed power-law dependence of total diffusion constant on tracer and matrix length relies on chemistry and reference temperature. However, if we can exclude localized contribution by tracking the diffusion of a monomer tracer, the hydrodynamic contribution should satisfy a universal expression.

From the above expression, the self-diffusion constant of a monodisperse unentangled polymer is predicted tobe

https://doi.org/10.1021/acs.macromol.5c02590
Macromolecules XXXX, XXX, XXX−XXX

$$D_{self} = \frac{D_{mono}}{N_{tra}} + 0.196\frac{k_BT}{R_{tra}N_{tra}\eta_0} \quad (21)$$

The hydrodynamic part is proportional to $N_{tra}^{-3/2}$. Thus, in the unentangled regime, the overall self-diffusion constant should scale with chain length with an exponent between − 3/2 and − 1. The exponent of self-diffusion in the entangled regime is predicted to be − 2 by the tube model.[19] Consequently, an exponent value slightly smaller than − 1 could have been recognized as the crossover from unentangled to entangled regimes in the existing literature.

III. MOMENTUM-CONSERVING MD SIMULATIONS OF THE TRACER'S C.M. DIFFUSION

III.1. Simulation Methods. The above theoretical predictions are then compared with the MD simulation data. The classic KG model is used for simulation.[29] The monomers of the polymer chain are coarse-grained beads interacting with each other via the repulsive 6−12 Lennard-Jones (LJ) potential: $U_{LJ}(r) = 4\varepsilon[(r/\sigma)^{-12} - (r/\sigma)^{-6}]$. Quantities are expressed relative to the length and energetic parameters in the LJ potential. In this study, two sets of simulation data are examined. One has pure repulsive beads with a cutoff distance of $r_c = 2^{1/6}$. The other includes attractive interactions by setting the cutoff distance to $r_c = 2.50$. The bonded pairs are connected by a finitely extensible bond potential: $U_{FENE}(r) = -kR_m^2/2 \ln[1 - (r/R_m)^2]$ for $r < R_m$, where $k = 30$ and $R_m = 1.50$. All simulations are performed with LAMMPS.[48] All supplementary discussions on simulation methods are provided in the Supporting Information (SI).

In the simulations, a total of 10^5 beads are placed in a periodic cubic box. The motions of the matrix molecules are integrated under the *NPT* ensemble, using the Nosé-Hoover (NH) thermostat and barostat. The constant pressure simulations are more relevant to experimental measurement. I compared the *NPT* simulation with other momentum-conserving simulations, using the NH thermostat or the dissipative particle dynamics (DPD) thermostat under the constant-volume ensemble. It is found that these simulation methods generate almost identical results, as shown in Figure S1 of SI. The NH thermostat and barostat conserve the total momentum of the simulation if it is set to zero in the initial snapshot.[49] To prove that, the total c.m. motion of the simulation box is monitored, and no drift is observed, as illustrated in Figure S2. The target static pressure is set to $P = 5.0$ for repulsive beads. Under this pressure and a reduced temperature $k_BT = 1.0$, the average monomer's mass density in the long-chain limit is $\langle\rho_{mass}\rangle \approx 0.85$ with a fluctuation of $\langle\delta\rho_{mass}^2\rangle^{1/2} \approx 5 \times 10^{-4}$ (the mass of a bead is $m = 1.0$ and thus the mass density is equal to the number density). For attractive beads, the target pressure is set to $P = 0.0$. The corresponding density and fluctuation are $\langle\rho_{mass}\rangle \approx 0.89$ and $\langle\delta\rho_{mass}^2\rangle^{1/2} \approx 6 \times 10^{-4}$.

The equations of state of the simulation models are examined for their glass transition behaviors, which is shown in **Section B** of SI. The KG model with repulsive chains is widely used as a standard simulation model in the community. However, it is also known to exhibit unusual glass transition behavior. The coherent energy between monomers is necessary to show qualitatively similar glass transition as experimental data.[50] Although the VHI theory does not involve any glass transition property, testing in the two sets of simulation data will show the robustness of the theoretical argument and the validity of the simulation model. Because the chain models are flexible, the glass transition temperature only shows a weak dependence on the chain length under a fixed pressure, in agreement with previous simulation studies on a similar model.[51,52] In the rest of the discussions, a fixed temperature $k_BT = 1.0$ (iso-Tmp) is used for repulsive chains, which almost reminisces the iso-T_g condition. For attractive chains, I adopt a condition where a monomer tracer has the same diffusion constant (iso-D_{mono}). As mentioned previously, this condition should indicate an identical normalized monomeric interaction. Under this condition, the change of tracer's diffusion with the matrix will directly indicate a deviation from the Rouse dynamics. It is not consistent with the iso-T_g condition. The corresponding temperatures are $k_BT = 0.75$, 0.88, 0.95 for $N_{mat} = 2$, 5, 10, respectively, and $k_BT = 1.0$ for $N_{mat} \geq 20$.

In this study, the length of tracer is varied as $N_{tra} = 20$, 50, 100, and 200. The matrix chain length N_{mat} ranges from 2 to 200. The size of the longest tracer satisfies $R_{tra} < L/2$, where $R_{tra} = \sqrt{\langle R_{tra}^2\rangle}$ represents the root of mean-squared end-to-end distance and L is the length of simulation box. For the flexible KG simulation model, the number of beads per entanglement is $N_{eb} \approx 65 \pm 7$.[53] Thus, our discussions will cover the entire unentangled regime. The repulsive and attractive polymers have similar monomer density, and thus, their entanglement properties are also close to each other. The linear relaxation modulus and zero-shear-rate viscosity of the matrices are shown in Figure S4. The linear relaxation modulus of the matrix $E_{mat}(t)$ is measured from the time-correlation function of the stress component based on the Green−Kubo relation. The zero-shear-rate viscosity η_{mat} is the plateau value of the transient viscosity $\eta_{mat}^*(t) = \int_0^t dt E_{mat}(t)$. The crossover from the unentangled to entangled regime is identified from the matrix viscosity, as shown in Figure S5(a). Below the onset of entanglement, the viscosity grows linearly with the chain length in the iso-Tmp repulsive chains. The relaxation times of the tracer and matrix chains, τ_{tra} and τ_{mat}, are calculated from the time correlation function of the end-to-end vector. The correlation function is fitted via the exponential decay function: $\langle \boldsymbol{R}_{mat}(t) \cdot \boldsymbol{R}_{mat}(0)\rangle \sim \exp(-t/\tau_{mat})$. The corresponding value of τ_{mat} are presented in Figure S5(b), which also agrees with the unentangled to entangled transition. In repulsive chains, the best-fit values of the monomeric viscosity and relaxation time is $\eta_0 = \eta_{mat}/N_{mat} \approx 0.781$ and $\tau_0 = \tau_{mat}/N_{mat}^2 \approx 0.883$.

Tracer's c.m. diffusion is measured at different concentrations to identify the dilute regime. This step is tested in the matrix of $N_{mat} = 2$, where the tracer takes a swollen configuration. This test will give a safe estimation of the dilute regime in a θ solvent. The corresponding data are presented in Figure S6. The critical concentration of the dilute regime is found to be $c/c^* \approx 0.330$, where $c^* = N_{tra}/R_{tra}^3$ is the theoretical overlap concentration. It corresponds to a critical volume fraction of 2.5% for the tracer $N_{tra} = 100$ and 1.4% for $N_{tra} = 200$. For the simulation data to be presented later, the tracer's volume fraction is set to 2% for $N_{tra} \leq 100$ and 1% for $N_{tra} = 200$.

III.2. Tracer's Size in Different Matrices. Before discussing tracer's diffusion, it is worth noting the change of tracer's size in different matrices. The classic Flory's mean-field theorem for excluded volume interaction[54] predicts that, when $N_{mat} \ll N_{tra}^{1/2}$, the matrix will be a good solvent to the tracer. The tracer swells with the decrease of matrix chain as $R_{tra} \sim N_{mat}^{-1/5}$. When $N_{mat} \gg N_{tra}^{1/2}$, the matrix is a θ solvent and the tracer's size is independent of the matrix chain length. However, experimental and simulation data from literature[55,56] have

https://doi.org/10.1021/acs.macromol.5c02590
Macromolecules XXXX, XXX, XXX−XXX

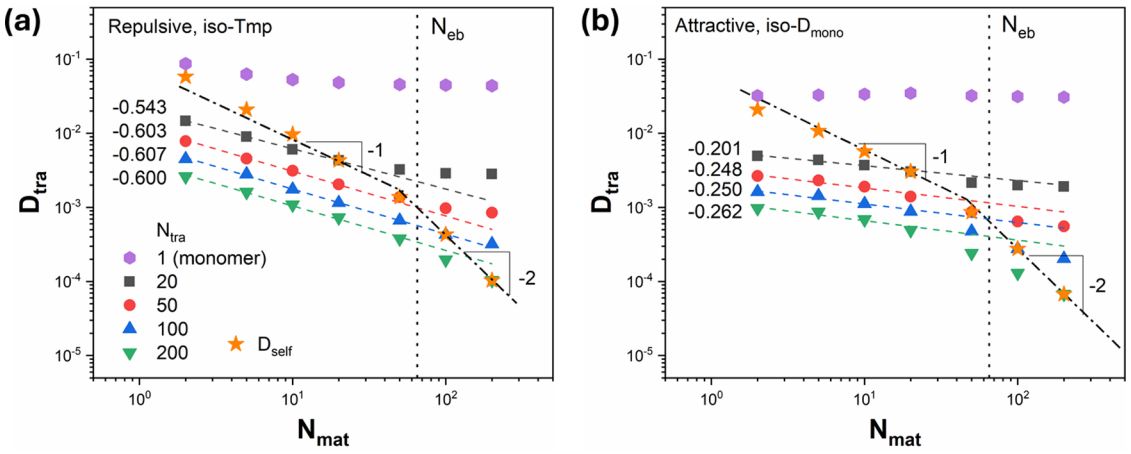

Figure 2. C.m. diffusion constants in the Fickian regime D_{tra} of a fixed tracer as a function of the matrix chain length N_{mat} with (a) repulsive and (b) attractive interaction. The vertically dotted line represents the entanglement length N_{eb}. The dashed lines are the best fits of the power-law function in the range of $N_{mat} \leqslant \min(N_{tra}, N_{eb})$, with the values of the exponent shown in the figure. The star scatters represent the self-diffusion constant in the monodisperse melt, $N_{tra} = N_{mat}$. The dash-dot lines with the slope of −1 and −2 are the predictions of the Rouse model and reptation model for unentangled and entangled dynamics, respectively.

reported a much weaker dependence in the good solvent regime: $R_{tra} \sim N_{mat}^{-0.1}$. The disagreement has been addressed by Lang et al.[56] who took into account of the long-range bond correlations in polymer melt and corrections to excluded volume. In my simulation data with a tracer length $N_{tra} = 200$, the relation $R_{tra} \sim N_{mat}^{-0.1}$ is reproduced. The corresponding data of tracer's size are plotted in **Figure S6**(a). The θ to good solvent transient is also tracked from the dependence $R_{tra} \sim N_{tra}^{\nu}$, and the change of ν from 1/2 to 3/5 is well confirmed, as shown in Figure S6(b).

To derive the hydrodynamic diffusion constant $D_h^*(t)$ in eqn 14, no excluded volume interaction is assume, i.e., $R_{tra} = N_{tra}^{1/2} b$. However, eqn 14 remains valid even though the θ to good solvent transient with the decrease of matrix chain length. The Zimm model predicts the same scaling expression for the diffusion constant in a good solvent, and the numerical factors are also very similar (0.203 for good solvent compared to 0.196 for θ solvent).[19]

III.3. Tracer's C.M. Diffusion in the Fickian Regime from Simulations. The tracers' c.m. diffusion constants in the Fickian regime D_{tra} in different matrices are summarized in Figure 2. First, for the monomer tracer, or saying $N_{tra} = 1$, a weak dependence on the matrix is observed in iso-Tmp repulsive chains when $N_{mat} \leqslant 10$. The main factor is the change of density with chain length under constant pressure. This effect is corrected in the attractive chains, as shown in Figure 2(b). For polymer tracers in unentangled matrices $N_{mat} \leqslant N_{eb}$, a power-law relationship is found $D_{tra} \sim N_{mat}^{-0.543}$ for the short tracer $N_{tra} = 20$, and $D_{tra} \sim N_{mat}^{-0.60}$ for longer tracers $N_{tra} \geqslant 50$ in the repulsive system. In the attractive system, weaker dependences are found: $D_{tra} \sim N_{mat}^{-(0.201 - 0.262)}$ after the iso-D_{mono} correction. It shows that the decrease of D_{tra} in Figure 2(a) is partly due to the change of monomeric potential in different matrices. But it is still necessary to include other mechanisms to describe the data. The simulation data is within the theoretical prediction of eqn 20. This indicates that the matrix dependence of tracer's c.m. diffusion in the unentangled regime is neither purely Rouse-like nor purely Zimm-like, but exhibits an intermediate behavior between the two limits.

In entangled matrices, the diffusivity of the tracer is determined by its entanglement state. The diffusion constant of an unentangled tracer (e.g., $N_{tra} = 20$) is nearly independent of the matrix chain size in the entangled regime. In contrast, D_{tra} of an entangled tracer (e.g., $N_{tra} = 200$) drops significantly with N_{mat} when $N_{mat} > N_{eb}$, indicating the effect of topological interaction. The transition from the unentangled to entangled regime can also be noted from the self-diffusion constants D_{self} in the monodisperse melts, which are also plotted in Figure 2. The two classic dependences, $D_{self} \sim N_{tra}^{-1}$ for the unentangled regime, and $D_{self} \sim N_{tra}^{-2}$ for the entangled regime, well approximate our simulation data. Meanwhile, it is also noticed that in the unentangled regime, the exponent describing the chain-length dependence of D_{self} is slightly smaller than − 1. This deviation is predicted by eqn 21 as the superposition of the Rouse-like and the Zimm-like processes.

Figure 3 plots the tracer's diffusion constants as a function of tracer's size for different tracers in the same matrix. In the unentangled matrices of repulsive beads, the dependence changes from $D_{tra} \sim R_{tra}^{-1.206}$ for $N_{mat} = 2$, which is close to the Zimm model, to $D_{tra} \sim R_{tra}^{-1.738}$ for $N_{mat} = 50$. An exponent consistent with the Rouse model is observed only when the

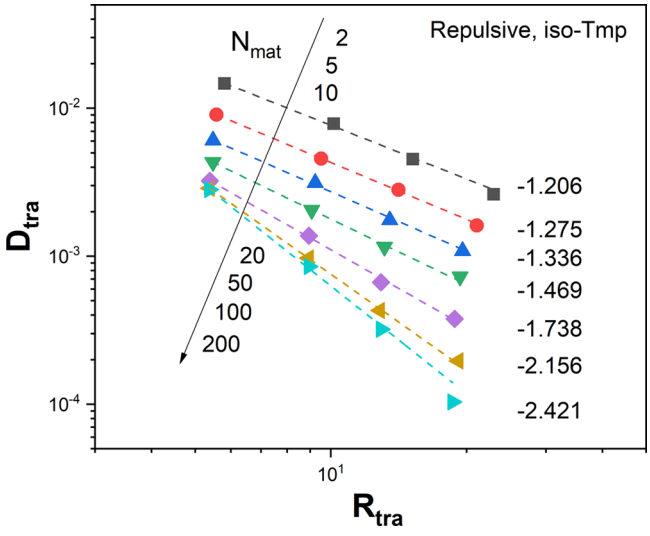

Figure 3. C.m. diffusion constants D_{tra} of different tracers diluted in the same matrix as a function of the tracer's size R_{tra}.

https://doi.org/10.1021/acs.macromol.5c02590
Macromolecules XXXX, XXX, XXX−XXX

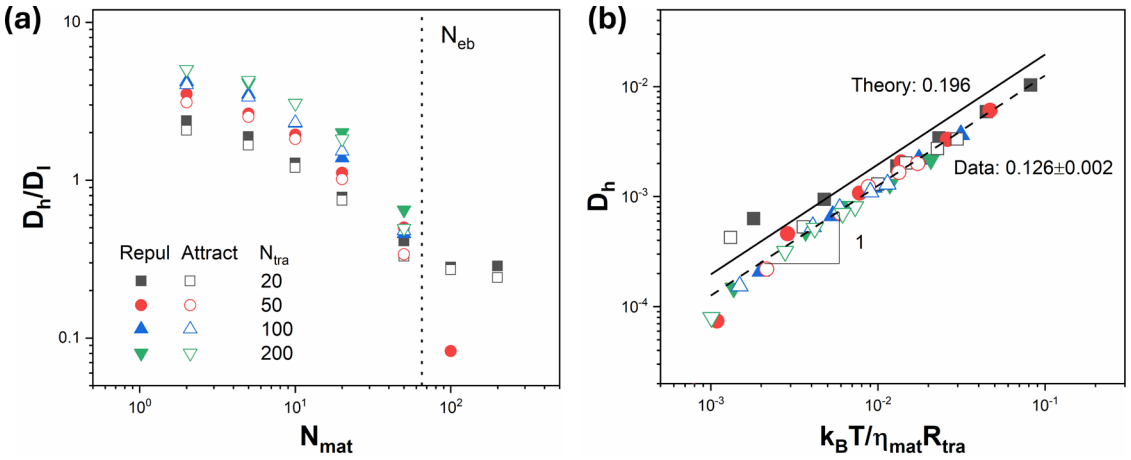

Figure 4. (a) Ratio of the hydrodynamic and localized contributions to the tracer's c.m. diffusion. The localized diffusion constant is based on the diffusion of the monomer tracer in the same matrix, $D_l = D_{mono}/N_{tra}$, as shown in eq 12. The hydrodynamic diffusion constant is the difference between the total diffusion and the localized diffusion, $D_h = D_{tra} - D_l$. (b) Hydrodynamic diffusion constant D_h compared to the theoretical prediction of eq 20. The solid and dashed lines represent the linear relation. The theory predicts a numerical coefficient of 0.196. The best fit value of the simulation data (short tracers in the longer matrices excluded) is 0.126 ± 0.002.

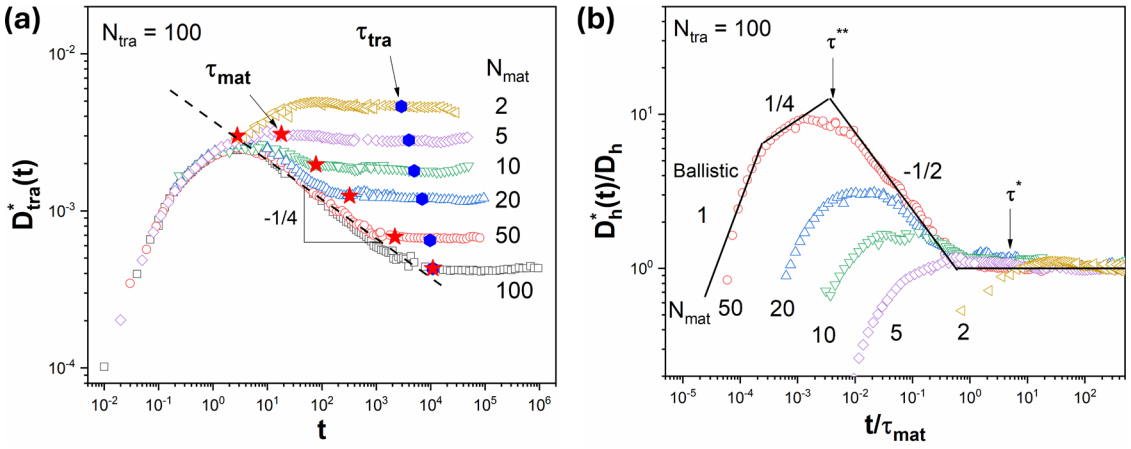

Figure 5. (a) Transient c.m. diffusion constants $D^*_{tra}(t) = \partial g_3(t)/6\partial t$ for the tracer of fixed length N_{tra} = 100 in different matrices with repulsive interaction. The blue-hexagonal and red-star scatters represent the end-to-end relaxation time of the tracer and matrix chains, τ_{tra} and τ_{mat}, respectively. (b) Transient hydrodynamic diffusion constants normalized by the corresponding values in the Fickian regime, $D^*_h(t)/D_h$, as a function of time normalized by the matrix chain relaxation time, t/τ_{mat}. The solid lines with different power-law relations are the prediction of the VHI theory in eqn 19. The other crossover times from the predictive expressions are shown in the figure (τ^* for N_{tra} = 2 and τ^{**} for N_{tra} = 50).

matrix chains are near the onset of entanglement. The plot further proves that tracer's c.m. diffusion in the unentangled matrix always superposes the Rouse and Zimm dynamics, in agreement with the VHI theory proposed in this work. When the matrix is entangled, the exponent value becomes smaller than −2.

The hydrodynamic contribution of the c.m. diffusion is further highlighted to compare with the theory. The localized part of diffusion constant for the polymer tracer is $D_l = D_{mono}/N_{tra}$ from eqn 12. The hydrodynamic contribution is calculated as the difference between the total diffusion and the localized diffusion, $D_h = D_{tra} - D_l$. The simulation data confirms that the localized contribution is insufficient to predict the total diffusion, and the hydrodynamic diffusion in the unentangled matrix is always nontrivial. Figure 4(a) presents the ratio of the hydrodynamic and localized diffusion constants, D_h/D_l. In the short-chain matrix, the hydrodynamic part is more important. The value of D_h/D_l also increases with the tracer's length N_{tra}. D_h/D_l decreases as the matrix chain length increases, and beyond a certain point, the localized contribution overwhelms the hydrodynamic part. However, D_h remains non-negligible throughout the entire unentangled regime. Even near the onset of entanglement ($N_{tra} = N_{mat} = 50$), D_h/D_l is found to be 0.502. When the matrix becomes entangled, the total diffusion of a long tracer that can be entangled with the matrix (e.g., $N_{tra} \geqslant 100$) is smaller than the localized diffusion from the monomer tracer. Thus, it results in a negative value of the apparent hydrodynamic diffusion.

The hydrodynamic diffusion constants D_h in Figure 4(a) are plotted with the Zimm-like prediction $k_BT/\eta_{mat}R_{tra}$ in Figure 4(b). The simulation data exhibits excellent agreement with the theoretical prediction, regardless of the monomer's interaction. Moreover, the numerical factor from the current simulations has the same order of magnitude as Zimm's theory, although smaller by 36% (0.126 ± 0.002 compared to 0.196). There are several explanations for the difference in numerical factors. One is the finite size effects in simulations. When simulating a fluid with periodic boundary condition, the diffusion constant is under-

https://doi.org/10.1021/acs.macromol.5c02590
Macromolecules XXXX, XXX, XXX−XXX

estimated and converges as $1/L$.[57] Meanwhile, it must be noted that the experimental data in small-molecule θ solvents reported a numerical factor around 15% smaller than the prediction.[19] Thus, there are also physical origins of the discrepancy, like non-Gaussian distribution and hydrodynamic fluctuation.[19] In spite of these factors, the general agreement among theory, experiments and simulations is remarkable. The main finding of this study is that the consistency can still hold even if an unentangled polymer melt is used as the solvent, provided that the localized contribution is carefully estimated.

For a short tracer ($N_{tra} = 20$) in a longer matrix ($N_{mat} = 100$ or 200), a finite value of D_h is found. It is independent of the matrix and larger than $k_BT/\eta_{mat}R_{tra}$ with the best-fit numerical coefficient. The result supports the idea that in the Fickian regime, the HI for a short tracer in a long matrix is still not screened but coupled with an effective viscosity smaller than the bulk matrix viscosity, $\eta_{eff} < \eta_{mat}$. The simulation data show that the prefactor should be $\eta_{eff}/N_{tra}\eta_0 \approx 2.103$. It suggests that a tracer can be coupled with a matrix strand up to twice its own length, consistent with the simple scaling argument.

III.4. Tracer's C.M. Diffusion in the Transient Regime. Direct evidence of the VHI in unentangled polymer is also identified from the tracer's transient diffusion before reaching the Fickian diffusion regime. In the simulations, the transient diffusion constants are calculated as the time derivative of the c.m. MSD, $D^*_{tra}(t) = \partial g_3(t)/6\partial t$. Figure 5(a) plots $D^*_{tra}(t)$ for a fixed tracer of $N_{tra} = 100$ in different matrices with repulsive interaction. The matrix and tracer relaxation times, τ_{mat} and τ_{tra}, are marked in the figure for clarity.

Qualitatively different behaviors of $D^*_{tra}(t)$ are found when varying the lengths of matrix chains, consistent with the VHI theory prediction in Figure 1(b). In the matrix of very short chains, e.g., $N_{mat} = 2$, $D^*_{tra}(t)$ increases monotonically with time. Fickian diffusion is onset at a time between τ_{mat} and τ_{tra}. Beyond a certain matrix chain length, we will find a regime where $D^*_{tra}(t)$ decreases with time as $D^*_{tra}\sim t^{-1/4}$, which means a subdiffusion $g_3\sim t^{3/4}$. The theory predicts that whether the tracer contains a subdiffusion regime is determined by the factor $N_{mat}/N_{tra}^{1/3}$, as shown in eqn 15. Substituting the corresponding values of the simulation model into eqn 15 ($b \approx 1.80$, $\rho_{mass} \approx 0.85$, $\tau_0 \approx 0.883$ and $\eta_0 \approx 0.781$), it shows that for a tracer of $N_{tra} = 100$, the critical matrix chain length is around 6. The theoretical expression excellently predicts the simulation data, where the critical matrix length is close to 5, as shown in Figure 5(a). Subdiffusion occurs when $N_{mat} \geq 10$. In this case, the onset of Fickian diffusion is well consistent with the matrix relaxation time, in agreement with the theoretical prediction. In contrast, the tracer's relaxation time τ_{tra} is irrelevant to the transient behavior of $D^*_{tra}(t)$ except the cases of monodisperse melt.

To further compare with the theoretical prediction, we need to focus on the hydrodynamic contribution by subtracting the localized contribution from the total diffusion. Figure 5(b) plots the transient hydrodynamic diffusion constant normalized by the corresponding values in the Fickian regime, $D^*_h(t)/D_h$, as a function of time normalized by the matrix chain relaxation time t/τ_{mat}. In this figure, the scaling $D^*_h\sim t^{-1/2}$ following $D^*_h\sim t^{1/4}$ is well identified, in comparison to $D^*_{tra}\sim t^{-1/4}$ for the total diffusion. It further proves that, to obtain quantitative agreement with the VHI theory, the localized contribution of diffusion needs to be excluded from the total diffusion in general cases. At very short times, $D^*_h(t)$ belongs to the so-called ballistic regime and increases linearly with time. In this regime, the tracer has not felt the surrounding molecules. In the matrix of $N_{mat} = 50$, the crossover from $D^*_h\sim t^{1/4}$ to $D^*_h\sim t^{-1/2}$ is $\tau^{**}/\tau_{mat} \approx 0.0036$ by extrapolating the power-law regime in the simulation data. The predictive value for this characteristic time is $\tau^{**} \cong (\rho_{mass}\eta_0^{-1}\tau_0^{1/2}R_{tra}^2/6)^{2/3} \approx 9$ (a numerical factor of 1/6 is to replace end-to-end distance by radius of gyration as a more reasonable estimation of the tracer's size), corresponding to $\tau^{**}/\tau_{mat} \approx 0.0041$. The difference is quite small, as indicated in the figure. In shorter matrices with $N_{mat} = 20$ and 10, the regime showing $D^*_h\sim t^{1/4}$ is not very clear, and the crossover from a positive to a negative exponent is quite flat. The reason is that, for these short matrices, the Rouse-like description of transient viscosity, $\eta^*_{mat}(t) = \eta_{mat}(t/\tau_{mat})^{1/2}$ for $t \ll \tau_{mat}$, is not well satisfied. In the matrix of $N_{mat} = 2$ where $D^*_h(t)$ does not exhibit subdiffusion, the theoretical expression predicts that the onset of Fickian diffusion is $\tau^* \cong \rho_m R_{tra}^2/6\eta_{mat} \approx 15$, or $\tau^*/\tau_{mat} \approx 5$, in reasonable agreement with simulation data.

IV. DISCUSSIONS

IV.1. Tracer's Monomeric Diffusion. The influence of matrix chain size on tracer's monomeric diffusivity is also investigated. The monomeric MSD is defined as $g_1(t) \equiv \langle[r_i(t) - r_i(0)]^2\rangle$. The idea of thinking about monomeric diffusion is that by the time t, a monomer in the tracer chain can "feel" that it belongs to a strand whose relaxation time is equal to t.[1] Suppose that this strand consists of g monomers. For the Rouse model, $\tau_0 g^2 \cong t$, which means $g \cong (t/\tau_0)^{1/2}$ for $\tau_0 \ll t \ll \tau_{tra}$. Then the monomeric MSD is predicted tobe

$$g_1^{(R)}(t) \cong t\frac{k_BT}{\zeta g} \sim t^{1/2} \tag{22}$$

For the Zimm model, the relaxation time of the strand is $\tau_0 g^{3\nu} \cong \tau_0(\xi/b)^3 \cong t$, where $\xi \cong g^\nu b$ is the size of the strand. The corresponding monomeric MSD is

$$g_1^{(Z)}(t) \cong t\frac{k_BT}{\eta_S \xi} \sim t^{2/3} \tag{23}$$

The exponent value is independent of the solvent quality.

In a viscoelastic matrix, the theory proposed in this work suggests that the tracer's diffusion superposes Rouse-like and Zimm-like processes, originating from the localized and nonlocalized flow-to-force responses, respectively. Thus, it can be expected that the tracer's monomeric MSD in an unentangled matrix exhibits a power-law exponent between 1/2 and 2/3. The start of the scaling regime should be consistent with the Fickian regime of c.m. diffusion, so that the time-dependence of the matrix viscosity can be neglected, as assumed by the Rouse and Zimm models. For a matrix that is not too short, i.e., $N_{mat}/N_{tra}^{1/3} \gg 1$, it means $\tau_{mat} \ll t \ll \tau_{tra}$.

The exact exponent value of monomeric MSD can be predicted from the c.m. diffusion. The relaxation time of the strand of size $\xi \cong g^\nu b$ in the unentangled matrix is $\tau_g \cong \xi^2/D_g$, where D_g is the c.m. diffusion constant of this strand. In Figure 3 for c.m. diffusion, I have shown the power-law relation between D_g and the strand size for different tracers in a fixed matrix: $D_g \sim \xi^\alpha$, where $-1.206 \geqslant \alpha \geqslant -2.156$ for $2 \leqslant N_{mat} \leqslant 100$. Thus, if $\tau_g \cong t$, $\xi \sim t^{1/(2-\alpha)}$. The time dependence of monomeric MSD is

$$g_1(t) \cong \xi^2 \sim t^{2/(2-\alpha)} \tag{24}$$

The simulation data of tracer's monomeric MSD $g_1(t)$ for the fixed tracer of $N_{tra} = 100$ in different matrices with repulsive interaction is presented in Figure 6. The end-to-end relaxation

https://doi.org/10.1021/acs.macromol.5c02590
Macromolecules XXXX, XXX, XXX−XXX

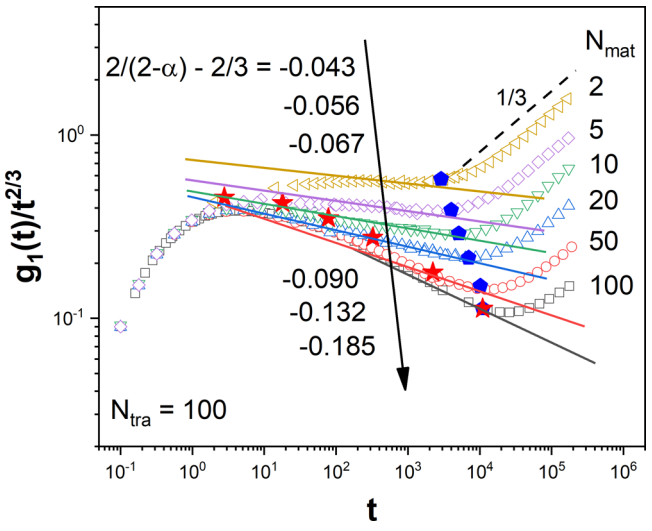

Figure 6. Simulation data of the tracer's monomeric MSD $g_1(t)$ divided by $t^{2/3}$ for the fixed tracer of N_{tra} = 100 in different matrices with repulsive interaction. The solid lines are the predictions of eqn 24, with the exponent value $2/(2-\alpha)-2/3$ ranging from −0.043 to −0.185. α is the exponent value describing the dependence $D_{tra}\sim R_{tra}^{\alpha}$, as shown in Figure 3. The dashed line with the exponent of 1/3 represents Fickian diffusion. Like Figure 5a, the blue-hexagonal and red-star scatters represent the end-to-end relaxation times of the tracer and matrix chains, τ_{tra} and τ_{mat}, respectively.

times of the tracer and matrix chains are also marked. When calculating $g_1(t)$ from simulations, I performed averaging over 10 monomers near the middle of the tracer chain. For clarity of the exponent value in the transient regime, $g_1(t)$ is divided by $t^{2/3}$. In this case, the horizontal line is the Zimm model prediction. The Rouse model prediction is represented by the exponent value $-1/6 \approx -0.167$. Fickian diffusion corresponds to an exponent of 1/3. In the simulations, unlike c.m. diffusion, the onset of Fickian monomeric diffusion is always consistent with the tracer's end-to-end relaxation time τ_{tra}. The simulation data lay between the Rouse and Zimm scaling when $t \ll \tau_{tra}$, as expected. Tracer's monomeric diffusion in the matrix of $N_{mat} = 2$ is very close to the Zimm-like scaling, showing a nearly plateau regime in Figure 6. The time dependence of $g_1(t)$ in longer matrices is always stronger than $t^{1/2}$ until the onset of entanglement ($N_{mat} > N_{eb} \approx 65$). Thus, the tracer's monomeric diffusion further supports that HI is a non-negligible factor in unentangled dynamics. Moreover, the exponent values agree well with the predictions of eqn 24, which are shown as solid lines in Figure 6. The results show that in the simulations the tracer's monomeric and c.m. diffusions in the unentangled matrix are well consistent with each other. It also proves that the theoretical argument about monomeric MSD based on the relaxation time of a strand is valid in general cases.

IV.2. Tracer's C.M. Diffusion Coupled with Langevin Thermostat. In MD simulations, it is common strategy to use the Langevin thermostat to mimic the effect of heat bath.[49] It introduces an additional friction force $\boldsymbol{f}_L = -\gamma m_i \boldsymbol{v}_i$ on the motion of particles, where γ is a damping parameter in the unit of frequency. With this thermostat, the initial momentum fluctuation is dissipated within the characteristic time γ^{-1}. The advantage of using the Langevin thermostat is that it can effectively equilibrate stiff degrees of freedom, and thus, it is more reliably ergodic.[49] However, the resulting dynamics is not momentum-conserving. As explained by Farago, Semenov et al.,[22,23] this artificial Langevin friction significantly modifies VHI. Here, I will explain its effect on tracer's diffusion in unentangled matrices. The objective of discussing this part is 2-fold: one is to further support the effect of VHI as the principal mechanism of the anomalous tracer's diffusion in unentangled regime; the second is to remind of the potential artifact when relating theory and experimental data from simulations.

The Langevin thermostat modifies the GNSE in eqn 3 by replacing $\rho_{mass}\partial \boldsymbol{v}(\boldsymbol{r},t)/\partial t$ with $\rho_{mass}(\partial/\partial t+\gamma)\boldsymbol{v}(\boldsymbol{r},t)$. If the length scale is much larger than the matrix chain, the generalized Oseen tensor $\mathcal{H}(r,t)$ can still be expressed as eqn 7, which is proportional to $1/r\eta^*_{mat}(t)$. But its validity is limited by not only the vorticity diffusion length $r < l^*_v(t) \cong \sqrt{t\eta^*_{mat}(t)/\rho_{mass}}$, but also an additional length scale, $r < l^*_L(t) \equiv \sqrt{\eta^*_{mat}(t)/\rho_{mass}\gamma}$, called the Langevin screening length. It defines the maximum length to which momentum can diffuse at time t due to the Langevin damping effect.[58] Unlike the vorticity length, the Langevin screening length does not increase to infinity at large times.

With the Langevin friction force, the time dependence of the transient hydrodynamic diffusion $D^*_h(t)$ can still be expressed in terms of the hydrodynamic screening length, as eqn 14. But here, we need to compare the tracer's size R_{tra} with two screening lengths, $l^*_v(t)$ and $l^*_L(t)$. Let us focus on the case of $N_{tra}^{1/3} \ll N_{mat} \ll N_{tra}$, where there is a subdiffusion regime and the onset of Fickian diffusion is determined by the matrix relaxation time τ_{mat} (**Case B** in **Section II.2**). The theoretical predictions are summarized as the following:

i) $t \ll \gamma^{-1}$**:** At such short times, the Langevin screening length $l^*_L(t)$ is larger than the vorticity diffusion length $l^*_v(t)$, so that we only need to consider hydrodynamic screening from $l^*_v(t)$. Thus, the tracer's c.m. diffusion will be the same as the momentum-conserving dynamics in this regime. Moreover, if $\gamma^{-1} \gg \tau_{mat}$, there is no difference between the two types of dynamics in the entire transient regime of tracer's diffusion. To observe the effect of the Langevin damping, it requires $\gamma \gg \tau^{-1}_{mat}$.

ii) $t \gg \gamma^{-1}$**:** Starting from the time γ^{-1}, $l^*_L(t)$ becomes the limiting parameter for tracer's diffusion. Like momentum-conserving dynamics, two conditions need to be considered. In the first condition, the Langevin screening length is smaller than the size of the tracer by the matrix relaxation time, $l^*_L(\tau_{mat}) \ll R_{tra}$, which means $\gamma \gg \eta_{mat}/(\rho_{mass}R^2_{tra})$. The transient hydrodynamic diffusion constant $D^*_h(t)$ is expressed as

$$D^*_h(t) \cong \frac{k_BT}{R^2_{tra}}\frac{l^*_L(t)}{\eta^*_{mat}(t)},\ t \gg \gamma^{-1} \tag{25}$$

for $\gamma \gg \max[\tau^{-1}_{mat}, \eta_{mat}/(\rho_{mass}R^2_{tra})]$. It can be expanded as

$$D^*_h(t) \sim \begin{cases} N^{-1}_{tra}t^{-1/4} & \gamma^{-1} \ll t \ll \tau_{mat} \\ N^{-1}_{tra}N^{-1/2}_{mat} & t \gg \tau_{mat} \end{cases} \tag{26}$$

In this case, the onset of Fickian diffusion is controlled by the matrix relaxation time τ_{mat}. Before that, $D^*_h(t)$ decreases with time, showing the power law of −1/4. The Fickian diffusion at large times is Rouse-like since it is inversely proportional to the tracer's length.

If $\gamma \ll \eta_{mat}/(\rho_{mass}R^2_{tra})$, the Langevin screening length becomes comparable to the tracer's size at a time smaller than the matrix relaxation time, $l^*_L(\overline{\gamma}\tau_{mat}) \cong R_{tra}$, where $\overline{\gamma} \cong (R^2_{tra}\rho_{mass}\gamma/\eta_{mat})^2 \ll 1$. The condition $\gamma \gg \tau^{-1}_{mat}$ can still

https://doi.org/10.1021/acs.macromol.5c02590
Macromolecules XXXX, XXX, XXX−XXX

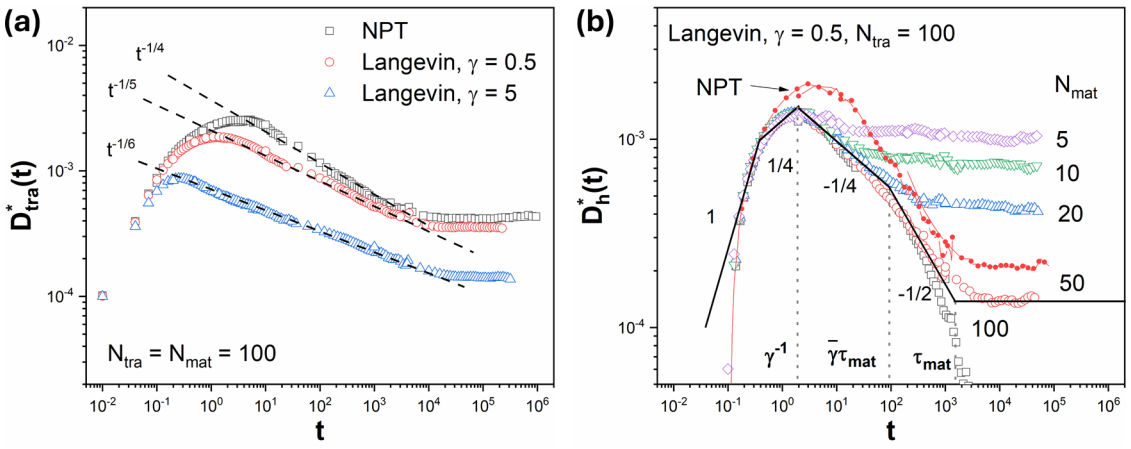

Figure 7. (a) Comparison of the tracer's total c.m. diffusion constants in the monodisperse melt $N_{tra} = N_{mat} = 100$ with repulsive chains, from momentum-conserving (*NPT*) and nonmomentum-conserving (Langevin with $\gamma = 0.5$ and 5) simulations of the same model. The exponents values for the subdiffusion regime are crude estimations of simulation data. (b) Matrix effect on the transient hydrodynamic diffusion constant for a fixed tracer $N_{tra} = 100$. The line-scatter plot is the data from *NPT* simulation of $N_{mat} = 50$.

be satisfied, because $N_{mat}^3/N_{tra} \gg \rho_{mass} b^2/\eta_0\tau_0$ is assumed. The transient hydrodynamic diffusion constant is expressed as

$$D_h^*(t) \cong \frac{k_BT}{R_{tra}} \begin{cases} l_L^*(t)/\eta_{mat}^*(t) R_{tra} & t \ll \overline{\gamma}\tau_{mat} \\ 1/\eta_{mat}^*(t) & \overline{\gamma}\tau_{mat} \ll t \ll \tau_{mat} \\ 1/\eta_{mat} & t \gg \tau_{mat} \end{cases} \quad (27)$$

for $\tau_{mat}^{-1} \ll \gamma \ll \eta_{mat}/(\rho_{mass} R_{tra}^2)$. The detailed dependences of $D_h^*(t)$ are

$$D_h^*(t) \sim \begin{cases} N_{tra}^{-1} t^{-1/4} & \gamma^{-1} \ll t \ll \overline{\gamma}\tau_{mat} \\ N_{tra}^{-1/2} N_{mat}^{-1} t^{-1/2} & \overline{\gamma}\tau_{mat} \ll t \ll \tau_{mat} \\ N_{tra}^{-1/2} N_{mat}^{-1} & t \gg \tau_{mat} \end{cases} \quad (28)$$

Thus, $D_h^*(t)$ contains two negative power-law regimes with time before Fickian diffusion: $D_h^*(t) \sim t^{-1/4}$ followed by $D_h^*(t) \sim t^{-1/2}$.

The predictions are compared with simulation data. In Figure 7(a), I first compare the tracer's c.m. total diffusion constants in the monodisperse melt, $N_{tra} = N_{mat} = 100$, from momentum-conserving (*NPT*) and nonmomentum-conserving simulations (Langevin) of the same model. The Langevin simulations are performed at constant density $\rho_{mass} = 0.85$. The damping parameters are set to $\gamma = 0.5$ and 5 in the Langevin simulations. The comparison confirms that tracer's c.m. diffusion is significantly modified in the presence of the Langevin damping effect. The Fickian diffusion constant decreases with the damping parameter. In the transient regime, the maximum of $D_{tra}^*(t)$ occurs at a smaller time compared to momentum-conserving simulations. The subdiffusion regime persists, but the Langevin simulations exhibit a weaker time dependence. The magnitude of the exponent decreases as the damping parameter increases.

I measured the diffusions of a monomer tracer and a polymer tracer of $N_{tra} = 100$ in different matrices with the Langevin thermostat. Like the simulations discussed previously, the hydrodynamic contribution of diffusion $D_h^*(t)$ is obtained by subtracting the localized contribution based on the diffusion of the monomer tracer from the total diffusion of the polymer tracer. The results of $D_h^*(t)$ are presented in Figure 7(b). The data is also compared with the momentum-conserving simulation. With the Langevin damping $\gamma = 0.5$, the maximum of $D_h^*(t)$ occurs at $t \approx 2 = \gamma^{-1}$, in agreement with the prediction.

For the subdiffusion regime, where $D_h^*(t)$ decreases with time, the theory predicts two qualitatively different behaviors, depending on the damping parameter, the tracer's size and the matrix viscosity (whether $\overline{\gamma} \cong (R_{tra}^2 \rho_{mass}\gamma/\eta_{mat})^2$ is larger than 1 or not). For the simulation parameters discussed in Figure 7(b), in the long matrix like $N_{mat} = 50$ or 100, $\overline{\gamma}$ is in the order of unit. The theory predicts a change of power-law exponent with time, from $D_h^*(t) \sim t^{-1/4}$ to $D_h^*(t) \sim t^{-1/2}$, as shown in eqn 28. In the simulation data, this enhanced time dependence is observed. In comparison, the *NPT* simulation is effectively described as a single dependence, $D_h^*(t) \sim t^{-1/2}$. In a short matrix like $N_{mat} = 20$, $\overline{\gamma}$ becomes much larger than 1. For this case, the theory predicts only one power-law regime $D_h^*(t) \sim t^{-1/4}$ before reaching the plateau, as shown in eqn 26, which also agrees with the simulation data.

V. CONCLUSIONS

In summary, the current study reported unambiguous evidence that HI is non-negligible in unentangled polymer melts, by tracking the diffusion of a polymer tracer in the matrices of different chain lengths. The so-called viscoelastic hydrodynamic interaction (VHI), as proposed by Farago, Semenov et al.[22,23] some years ago, was accounted for via the time-dependent generalized Oseen tensor derived from the GNSE for incompressible viscoelastic fluid. The current study explained the predictive theory of the matrix effect on tracer's diffusion in the unentangled regime regarding VHI. The theory decoupled the total tracer's c.m. diffusion constant $D_{tra}^*(t)$ into the localized and the hydrodynamic contributions, $D_l^*(t)$ and $D_h^*(t)$. One essential argument of this study was to describe the localized contribution, which is chemistry-dependent, as the diffusion of a monomer tracer in the polymer matrix. When $N_{tra} \gg N_{mat}$, the qualitative feature of the hydrodynamic contribution $D_h^*(t)$ in the transient regime was predicted to rely on the parameter $N_{mat}/N_{tra}^{1/3}$. This parameter determines whether momentum can spread over the entire chain before the full relaxation of the matrix chains. For $N_{mat}/N_{tra}^{1/3} \ll 1$, $D_h^*(t)$ increases monotonically with time. When $N_{mat}/N_{tra}^{1/3} \gg 1$, a subdiffusive regime was predicted, and the transient hydrodynamic diffusion scales as

https://doi.org/10.1021/acs.macromol.5c02590
Macromolecules XXXX, XXX, XXX−XXX

$D_h^*(t) \sim N_{tra}^{-1/2} N_{mat}^{-1} t^{-1/2}$ in this regime. The onset of Fickian diffusion is controlled by the matrix relaxation time. At large times, the theory proposed a formula that superposes the Rouse-like and Zimm-like processes for tracer's c.m. diffusion in the Fickian regime.

The predictions of the VHI theory were strongly supported by the momentum-conserving MD simulations that covered the entire range of unentangled polymers. By simulating the diffusions of the monomer tracer and the polymer tracer, and excluding the localized contribution from the total diffusion, the hydrodynamic diffusion constant in the Fickian regime exhibited excellent agreement with the Zimm-like expression, $D_h \cong k_B T/\eta_{mat} R_{tra}$, as predicted by the current theory. In the transient regime, simulations confirmed the qualitatively different profiles of $D_h^*(t)$ in different matrices, and the critical matrix chain length determining the shape of $D_h^*(t)$ was also consistent with the theory's prediction. The scaling dependence at different time scales as predicted by the theory was well identified in the simulation data. Further proofs of the VHI effect were discussed from the tracer's monomeric diffusion and the nonmomentum-conserving dynamics coupled with an artificial Langevin damping effect. The VHI theory, together with the simulation results, explains the experimental data on tracer diffusion in unentangled matrices, demonstrating that the classic Rouse description is insufficient for unentangled dynamics.

A direct test of the VHI theory from experiments is possible. The essential idea is to measure simultaneously the diffusions of a monomer tracer and a polymer tracer in the same polymer matrix, as performed in the simulations of this work. It is necessary to carefully exclude the localized contribution from the total diffusion to observe a Zimm-like dependence, because the localized and hydrodynamic contributions can be comparable with each other in the unentangled regime.

To this end, it is instructive to revisit the classic theory for unentangled polymer dynamics. The idea that HI is trivial in unentangled melts is extended from the concept of hydrodynamic screening in semidilute solutions. The key assumption of this picture is that the hydrodynamic screening length is proportional to the static concentration correlation length.[1] Thus, in a polymer melt or a concentrated solution, where the static correlation length is comparable to the size of a segment, HI is expected to be a trivial effect. However, there is no rigorous explanation why the simple proportionality between the hydrodynamic screening length and the static correlation length should hold at all concentrations. The proof of VHI effect suggests that this assumption should break at some point. Moreover, the time dependence of the hydrodynamic screening length is important in melts or concentrated solutions. Thus, the time-independent concentration correlation length is insufficient to describe the effect of VHI. A systematic investigation into the relation between the two length scales is an interesting subject to the current author for future studies.

The current work also provides significant insight into the recent active discussions on the nonlinear extensional rheology of unentangled polymers. The reduction of monomeric friction, which has been widely used as an explanation of nonlinear rheology and other related nonlinear phenomena when polymers are highly stretched, needs to be seriously revised, since its standpoint is the absence of long-range HI. If a polymer is deformed at the large scale, but remains undisrupted in its local scale, the effect of VHI should be the dominant factor to consider. In contrast, the localized flow-to-force response represented by the monomeric friction coefficient should remain unchanged. In this case, the related change of dynamic properties can be explained from a predictive theory. This subject will be systematically investigated in the follow-up studies.

■ ASSOCIATED CONTENT

Supporting Information

The Supporting Information is available free of charge at https://pubs.acs.org/doi/10.1021/acs.macromol.5c02590.

Comparison of momentum-conserving simulations and proof of no drift; glass transition of the simulation model; linear viscoelasticity and entanglement crossover of the matrix; effect of tracer's concentration; and tracer's size in different matrices (PDF)

■ AUTHOR INFORMATION

Corresponding Author

Nuofei Jiang − *Bio and Soft Matter, Institute on Condensed Matter and Nano-science, Université catholique de Louvain, Louvain-la-Neuve 1348, Belgium;* orcid.org/0000-0002-6105-354X; Email: nuofei.jiang@uclouvain.be

Complete contact information is available at: https://pubs.acs.org/10.1021/acs.macromol.5c02590

Notes

The author declares no competing financial interest.

■ ACKNOWLEDGMENTS

The author thanks Michael Rubinstein, Evelyne van Ruymbeke, and Quan Chen for the helpful discussions and invaluable comments. Computational resources have been provided by the Consortium des Équipements de Calcul Intensif (CÉCI), funded by the Fonds de la Recherche Scientifique de Belgique (F.R.S.-FNRS) under Grant No. 2.5020.11 and by the Walloon Region, and Lucia, the Tier-1 supercomputer of the Walloon Region, infrastructure funded by the Walloon Region under the grant agreement no. 1910247.

■ REFERENCES

(1) Rubinstein, M.; Colby, R. H. *Polymer physics*; Oxford University Press: New York, 2003.

(2) Watanabe, H.; Ishida, S.; Matsumiya, Y.; Inoue, T. Test of Full and Partial Tube Dilation Pictures in Entangled Blends of Linear Polyisoprenes. *Macromolecules* **2004**, *37* (17), 6619−6631.

(3) Van Ruymbeke, E.; Masubuchi, Y.; Watanabe, H. Effective Value of the Dynamic Dilution Exponent in Bidisperse Linear Polymers: From 1 to 4/3. *Macromolecules* **2012**, *45* (4), 2085−2098.

(4) Van Ruymbeke, E.; Shchetnikava, V.; Matsumiya, Y.; Watanabe, H. Dynamic Dilution Effect in Binary Blends of Linear Polymers with Well-Separated Molecular Weights. *Macromolecules* **2014**, *47* (21), 7653−7665.

(5) Ebrahimi, T.; Taghipour, H.; Grießl, D.; Mehrkhodavandi, P.; Hatzikiriakos, S. G.; van Ruymbeke, E. Binary Blends of Entangled Star and Linear Poly(hydroxybutyrate): Effect of Constraint Release and Dynamic Tube Dilation. *Macromolecules* **2017**, *50* (6), 2535−2546.

(6) Smith, B. A.; Samulski, E. T.; Yu, L.-P.; Winnik, M. A. Tube renewal versus reptation: polymer diffusion in molten poly (Propylene Oxide). *Phys. Rev. Lett.* **1984**, *52* (1), 45.

(7) Green, P. F.; Kramer, E. J. Matrix effects on the diffusion of long polymer chains. *Macromolecules* **1986**, *19* (4), 1108−1114.

(8) Von Seggern, J.; Klotz, S.; Cantow, H. J. Reptation and constraint release in linear polymer melts: an experimental study. *Macromolecules* **1991**, *24* (11), 3300−3303.

(9) Wang, S. Q. Chain dynamics in entangled polymers: Diffusion versus rheology and their comparison. *J. Polym. Sci., Part B: Polym. Phys.* **2003**, *41* (14), 1589−1604.
(10) Daoud, M.; De Gennes, P. G. Some remarks on the dynamics of polymer melts. *J. Polym. Sci.: Polym. Phys. Ed.* **1979**, *17* (11), 1971−1981.
(11) Brochard-Wyart, F.; Ajdari, A.; Leibler, L.; Rubinstein, M.; Viovy, J. L. Dynamics of stars and linear chains dissolved in a polymer melt. *Macromolecules* **1994**, *27* (3), 803−808.
(12) Graessley, W. W. Entangled linear, branched and network polymer systems — Molecular theories. In *Synthesis and Degradation Rheology and Extrusion*; Springer-Verlag: 1982; pp 67−117.
(13) Klein, J. Effect of matrix molecular weight on diffusion of a labeled molecule in a polymer melt. *Macromolecules* **1981**, *14* (2), 460−461.
(14) Klein, J. Dynamics of entangled linear, branched, and cyclic polymers. *Macromolecules* **1986**, *19* (1), 105−118.
(15) Wang, Z.; Larson, R. G. Constraint Release in Entangled Binary Blends of Linear Polymers: A Molecular Dynamics Study. *Macromolecules* **2008**, *41* (13), 4945−4960.
(16) Shanbhag, S.; Wang, Z. Molecular Simulation of Tracer Diffusion and Self-Diffusion in Entangled Polymers. *Macromolecules* **2020**, *53* (12), 4649−4658.
(17) Picu, R. C.; Rakshit, A. Coarse grained model of diffusion in entangled bidisperse polymer melts. *J. Chem. Phys.* **2007**, *127* (14), 144909.
(18) Raphaël, E.; Fredrickson, G. H.; Pincus, P. One long chain among shorter chains: the Flory approach revisited. *J. Phys. II France* **1992**, *2* (10), 1811−1823.
(19) Doi, M.; Edwards, S. F. *The theory of polymer dynamics*; Oxford University Press: New York, 1986.
(20) Farago, J.; Meyer, H.; Semenov, A. N. Anomalous Diffusion of a Polymer Chain in an Unentangled Melt. *Phys. Rev. Lett.* **2011**, *107* (17), No. 178301.
(21) Farago, J.; Semenov, A.; Meyer, H.; Wittmer, J.; Johner, A.; Baschnagel, J. Mode-coupling approach to polymer diffusion in an unentangled melt. I. The effect of density fluctuations. *Phys. Rev. E* **2012**, *85* (5), No. 051806.
(22) Farago, J.; Meyer, H.; Baschnagel, J.; Semenov, A. N. Mode-coupling approach to polymer diffusion in an unentangled melt. II. The effect of viscoelastic hydrodynamic interactions. *Phys. Rev. E* **2012**, *85* (5), No. 051807.
(23) Semenov, A. N.; Farago, J.; Meyer, H. Length-scale dependent relaxation shear modulus and viscoelastic hydrodynamic interactions in polymer liquids. *J. Chem. Phys.* **2012**, *136* (24), 244905.
(24) Paul, W.; Smith, G. D.; Yoon, D. Y.; Farago, B.; Rathgeber, S.; Zirkel, A.; Willner, L.; Richter, D. Chain motion in an unentangled polyethylene melt: A critical test of the rouse model by molecular dynamics simulations and neutron spin echo spectroscopy. *Phys. Rev. Lett.* **1998**, *80* (11), 2346−2349.
(25) Zamponi, M.; Wischnewski, A.; Monkenbusch, M.; Willner, L.; Richter, D.; Falus, P.; Farago, B.; Guenza, M. G. Cooperative Dynamics in Homopolymer Melts: A Comparison of Theoretical Predictions with Neutron Spin Echo Experiments. *J. Phys. Chem. B* **2008**, *112* (50), 16220−16229.
(26) Paul, W.; Smith, G. D. Structure and dynamics of amorphous polymers: computer simulations compared to experiment and theory. *Rep. Prog. Phys.* **2004**, *67* (7), 1117−1185.
(27) Morhenn, H.; Busch, S.; Meyer, H.; Richter, D.; Petry, W.; Unruh, T. Collective Intermolecular Motions Dominate the Picosecond Dynamics of Short Polymer Chains. *Phys. Rev. Lett.* **2013**, *111* (17), No. 173003.
(28) Aponte-Rivera, C.; Wijesekera, A. S.; Ge, T. Nanoparticle-Induced Hydrodynamic Flows in Unentangled Polymer Melts. *Macromolecules* **2025**, *58* (17), 9010−9017.
(29) Kremer, K.; Grest, G. S. Dynamics of entangled linear polymer melts: A molecular-dynamics simulation. *J. Chem. Phys.* **1990**, *92* (8), 5057−5086.
(30) Nielsen, J. K.; Rasmussen, H. K.; Hassager, O.; McKinley, G. H. Elongational viscosity of monodisperse and bidisperse polystyrene melts. *J. Rheol.* **2006**, *50* (4), 453−476.
(31) Huang, Q.; Alvarez, N. J.; Matsumiya, Y.; Rasmussen, H. K.; Watanabe, H.; Hassager, O. Extensional Rheology of Entangled Polystyrene Solutions Suggests Importance of Nematic Interactions. *ACS Macro Lett.* **2013**, *2* (8), 741−744.
(32) Huang, Q.; Mednova, O.; Rasmussen, H. K.; Alvarez, N. J.; Skov, A. L.; Almdal, K.; Hassager, O. Concentrated Polymer Solutions are Different from Melts: Role of Entanglement Molecular Weight. *Macromolecules* **2013**, *46* (12), 5026−5035.
(33) Costanzo, S.; Huang, Q.; Ianniruberto, G.; Marrucci, G.; Hassager, O.; Vlassopoulos, D. Shear and Extensional Rheology of Polystyrene Melts and Solutions with the Same Number of Entanglements. *Macromolecules* **2016**, *49* (10), 3925−3935.
(34) Shahid, T.; Clasen, C.; Oosterlinck, F.; van Ruymbeke, E. Diluting Entangled Polymers Affects Transient Hardening but Not Their Steady Elongational Viscosity. *Macromolecules* **2019**, *52* (6), 2521−2530.
(35) Matsumiya, Y.; Watanabe, H. Non-Universal Features in Uniaxially Extensional Rheology of Linear Polymer Melts and Concentrated Solutions: A Review. *Prog. Polym. Sci.* **2021**, *112*, No. 101325.
(36) Jiang, N.; van Ruymbeke, E. Variation of Spring Stiffness, Monomeric Friction, and Brownian Intensity in the Simulation System of Unentangled Melt under Steady Flow. *Macromolecules* **2023**, *56* (8), 2911−2929.
(37) Matsumiya, Y.; Watanabe, H.; Masubuchi, Y.; Huang, Q.; Hassager, O. Nonlinear Elongational Rheology of Unentangled Polystyrene and Poly(p-tert-butylstyrene) Melts. *Macromolecules* **2018**, *51* (23), 9710−9729.
(38) Ianniruberto, G.; Brasiello, A.; Marrucci, G. Modeling Unentangled Polystyrene Melts in Fast Elongational Flows. *Macromolecules* **2019**, *52* (12), 4610−4616.
(39) Jiang, N. Potential Universal Extensional Rheology in Concentrated Polymeric Liquids. *Macromolecules* **2024**, *57* (11), 5520−5532.
(40) Brochard Wyart, F.; de Gennes, P. G. Viscosity at small scales in polymer melts. *EPJ. E* **2000**, *1* (1), 93−97.
(41) Cai, L.-H.; Panyukov, S.; Rubinstein, M. Mobility of Nonsticky Nanoparticles in Polymer Liquids. *Macromolecules* **2011**, *44* (19), 7853−7863.
(42) Hansen, J.-P.; McDonald, I. R. *Theory of simple liquids: with applications to soft matter*; Academic Press: **2013**.
(43) Egorov, S. A. Anomalous nanoparticle diffusion in polymer solutions and melts: A mode-coupling theory study. *J. Chem. Phys.* **2011**, *134* (8), No. 084903.
(44) Yamamoto, U.; Schweizer, K. S. Theory of nanoparticle diffusion in unentangled and entangled polymer melts. *J. Chem. Phys.* **2011**, *135* (22), 224902.
(45) Holyst, R.; Bielejewska, A.; Szymański, J.; Wilk, A.; Patkowski, A.; Gapiński, J.; Żywociński, A.; Kalwarczyk, T.; Kalwarczyk, E.; Tabaka, M.; Ziębacz, N.; Wieczorek, S. A. Scaling form of viscosity at all length-scales in poly(ethylene glycol) solutions studied by fluorescence correlation spectroscopy and capillary electrophoresis. *Phys. Chem. Chem. Phys.* **2009**, *11* (40), 9025−9032.
(46) Yamamoto, U.; Schweizer, K. S. Microscopic Theory of the Long-Time Diffusivity and Intermediate-Time Anomalous Transport of a Nanoparticle in Polymer Melts. *Macromolecules* **2015**, *48* (1), 152−163.
(47) Zimm, B. H. Dynamics of polymer molecules in dilute solution: viscoelasticity, flow birefringence and dielectric loss. *J. Chem. Phys.* **1956**, *24* (2), 269−278.
(48) Thompson, A. P.; Aktulga, H. M.; Berger, R.; Bolintineanu, D. S.; Brown, W. M.; Crozier, P. S.; In't Veld, P. J.; Kohlmeyer, A.; Moore, S. G.; Nguyen, T. D.; Shan, R.; Stevens, M. J.; Tranchida, J.; Trott, C.; Plimpton, S. J. LAMMPS - a flexible simulation tool for particle-based materials modeling at the atomic, meso, and continuum scales. *Comput. Phys. Commun.* **2022**, *271*, No. 108171.

https://doi.org/10.1021/acs.macromol.5c02590
Macromolecules XXXX, XXX, XXX−XXX

(49) Allen, M. P.; Tildesley, D. J. *Computer simulation of liquids*; Oxford University Press: 2017.
(50) Binder, K.; Baschnagel, J.; Paul, W. Glass transition of polymer melts: test of theoretical concepts by computer simulation. *Prog. Polym. Sci.* **2003**, *28* (1), 115−172.
(51) Schnell, B.; Meyer, H.; Fond, C.; Wittmer, J. P.; Baschnagel, J. Simulated glass-forming polymer melts: Glass transition temperature and elastic constants of the glassy state. *Eur. Phys. J. E* **2011**, *34* (9), 97.
(52) Durand, M.; Meyer, H.; Benzerara, O.; Baschnagel, J.; Vitrac, O. Molecular dynamics simulations of the chain dynamics in monodisperse oligomer melts and of the oligomer tracer diffusion in an entangled polymer matrix. *J. Chem. Phys.* **2010**, *132* (19), 194902.
(53) Svaneborg, C.; Everaers, R. Characteristic Time and Length Scales in Melts of Kremer−Grest Bead−Spring Polymers with Wormlike Bending Stiffness. *Macromolecules* **2020**, *53* (6), 1917−1941.
(54) Flory, P. J. The Configuration of Real Polymer Chains. *J. Chem. Phys.* **1949**, *17* (3), 303−310.
(55) Landry, M. R. Scaling Behavior of Swollen Chains in Bimodal Molecular Weight Blends. *Macromolecules* **1997**, *30* (24), 7500−7510.
(56) Lang, M.; Rubinstein, M.; Sommer, J.-U. Conformations of a Long Polymer in a Melt of Shorter Chains: Generalizations of the Flory Theorem. *ACS Macro Lett.* **2015**, *4* (2), 177−181.
(57) Yeh, I.-C.; Hummer, G. System-Size Dependence of Diffusion Coefficients and Viscosities from Molecular Dynamics Simulations with Periodic Boundary Conditions. *J. Phys. Chem. B* **2004**, *108* (40), 15873−15879.
(58) Dünweg, B. Molecular dynamics algorithms and hydrodynamic screening. *J. Chem. Phys.* **1993**, *99* (9), 6977−6982.

https://doi.org/10.1021/acs.macromol.5c02590
Macromolecules XXXX, XXX, XXX−XXX